PCCP

COMMUNICATION

View Article Online
View Journal | View Issue

Cite this: *Phys. Chem. Chem. Phys.*, 2025, **27**, 5956

Received 8th February 2025,
Accepted 25th February 2025

DOI: 10.1039/d5cp00510h

rsc.li/pccp

Harnessing luminescence from a heavy-atom-free organic charge-transfer cocrystal†

Suvarna Sujilkumar and Mahesh Hariharan *

Harvesting luminescence from charge-transfer cocrystals is an efficient strategy for developing solid-state light-emitting materials without requiring the multistep organic synthesis. Herein, we report comprehensive single-crystal, computational, and spectroscopic investigations of a heavy-atom-free charge-transfer cocrystal exhibiting a 40.2% photoluminescence quantum yield.

The access to luminescence from organic chromophores has been a flourishing area of research that has given rise to a plethora of applications.[1–3] The conventional strategies employed to achieve bright orange-red-region luminescence in organic chromophores include aggregation,[4] use of covalently connected donor–acceptors,[5] host–guest architectures,[5] and supramolecular assembly.[6] However, the tedious efforts required in the synthesis and modifications of organic chromophores act as a hurdle to the facile achievement of efficiently luminescent materials. Noncovalently stacked donor–acceptor cocrystals exhibiting through-space charge transfer constitute a promising class of compounds for exciton generation from the charge-transfer (CT) state.[3,7] Accordingly, great efforts have been devoted to activating luminescence from CT cocrystals, where the halogens or heavy atoms plays a crucial role in stabilizing the crystal structure and furnishing the radiative process.[8] However, this strategy also leaves obstacles to overcome, specifically the high costs and toxicity of the materials used, demanding the quest for designing heavy-atom-free cocrystals exhibiting luminescence from the CT state.

Our long-standing efforts to develop beneficial crystal architectures and monitor the charge-transfer exciton dynamics have motivated us to design heavy-atom-free CT cocrystals to access luminescence from long-lived CT states.[9,10] Herein, we crystallized 1,6-bis(4,4,5,5-tetramethyl-1,3,2-dioxaborolan-2-yl)pyrene (PYDB) with 1,2,4,5-tetracyanobenzene (TCNB) to give a ···DADA··· mixed stack cocrystal, denoted as PYDB–TCNB, exhibiting a photoluminescence quantum yield of 40.2% in the orange-red region (Fig. 1). Fluorescence-lifetime-based imaging of the cocrystal aided the construction of an image based on the fluorescence lifetime of the PYDB–TCNB cocrystal. Quantum chemical calculations proved the critical role of noncovalent interactions between the donor and acceptor in enabling substantial through-space excitonic coupling and stabilizing the 3-dimensional (3D) assembly. We envisaged that the rate of fluorescence can be enhanced through these stabilizing interactions and effective excitonic coupling between donor and acceptor. The current work aimed to design and spectroscopically investigate heavy-atom-free cocrystals for potential applications in organic optoelectronics.

PYDB was synthesized and characterized according to the previously reported procedure (Fig. 1 and Scheme S1 and Fig. S1, S2, ESI†).[11] Diffraction-quality PYDB–TCNB cocrystals were obtained by

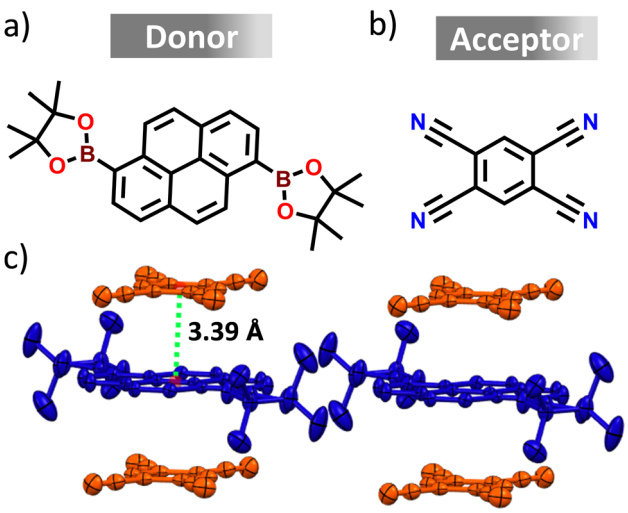

Fig. 1 Molecular structures of (a) PYDB (donor) and (b) TCNB (acceptor). (c) Crystal structure of PYDB–TCNB (unit cell) cocrystal and centroid-to-centroid distance (with the probability level of thermal ellipsoids being 30% and hydrogen atoms omitted for clarity).

School of Chemistry, Indian Institute of Science Education and Research Thiruvananthapuram, Maruthamala P.O., Vithura, Thiruvananthapuram, Kerala 695551, India. E-mail: mahesh@iisertvm.ac.in

† Electronic supplementary information (ESI) available. CCDC 2393609 and 2393610. For ESI and crystallographic data in CIF or other electronic format see DOI: https://doi.org/10.1039/d5cp00510h

carrying out a mechanochemical liquid-assisted grinding of a 1:2 ratio of PYDB and TCNB with a minimal amount of methanol, followed by dissolving in dichloromethane and layering the resulting solution with hexane (for details, see ESI,† Section B and Table S1). The presence of four cyano groups in the TCNB was deemed to make it a suitable candidate as an acceptor and to additionally facilitate π–π stacking and C–H···N interactions. Pyrene, being a donor with an extended π-conjugated skeleton and further decorated with boronic esters can enhance the crystallization tendency and form a strong CT complex with TCNB. Furthermore, the recorded infrared (IR) spectrum of the PYDB–TCNB cocrystal resembled a combination of the solid-state IR spectra of PYDB and TCNB, verifying the CT complexation (Fig. S3, ESI†). An analysis of the 3D crystal packing of the PYDB–TCNB cocrystal revealed co-facially aligned donor–acceptor stacking with a π–π stacking distance of 3.39 Å, which can facilitate efficient through-space charge transfer (Fig. 1). A comprehensive analysis of the 3D assembly of the cocrystal revealed additional stabilizing interstack C–H···H ($d_{C–H···H}$ = 2.38 Å), and intrastack C–N···H ($d_{C–N···H}$ = 2.82 Å) interactions (Fig. S4 and S5, ESI†). These interactions were posited to promote a close proximity between the donor and acceptor moieties and enhance the rate of radiative decay by preventing vibrational dissipation.[12] A Hirshfeld surface analysis was performed to obtain a statistical overview of the intermolecular interactions within the crystal assembly.[13] The acquired 2D fingerprint plots indicated a pivotal role played by H···H interactions, with a 55% contribution, followed by H···N (25.5%) and C···C interactions (8.7%) (Table S2 and Fig. S6, ESI†). A noncovalent interaction (NCI) analysis enabled a detailed visualization of noncovalent interactions in the molecules, specifically by analyzing the topology of the electron density, with green discs indicating stabilizing interactions and red discs signifying destabilizing interactions.[14] The presence of a green disc sandwiched between the donor and acceptor moieties suggested the occurrence of a stabilizing noncovalent interaction in the cocrystal (Fig. S7, ESI†). The detailed analysis of the cocrystal packing revealed, along with the co-facial donor–acceptor pair (DA1), two other types of donor–acceptor pairs, namely DA2 and DA3, with respective DA pair distances of 3.76 Å and 4.15 Å (Fig. S8, ESI†).

The truncated symmetry-adapted perturbation theory, commonly known as SAPT, is used to compute the interaction energy between two monomers and decompose it into physically meaningful components such as electrostatic, exchange, induction, and dispersion components. In the current work, SAPT(0), the simplest truncation of SAPT, was carried out for the three identified DA pairs using a 6-31G(d,p) basis set employing the Psi4 code.[15] According to the SAPT(0) analysis, for all three identified DA pairs, the dispersion energy was indicated to play a prevalent role in the stabilization of the 3D assembly, leading to a negative total SAPT(0) value (Table S3, ESI†). DA1 was identified as the most stable DA pair with $E^{SAPT(0)}$ = −85.61 kJ mol^{-1}, followed by DA2 ($E^{SAPT(0)}$ = −10.20 kJ mol^{-1}) and DA3 ($E^{SAPT(0)}$ = −4.42 kJ mol^{-1}). This stability trend was found to inversely correlate with the distance between the donor and acceptor.

Having elucidated the stabilizing nature of DA pairs in the formation of the 3D assembly, we set out to theoretically evaluate the excitonic coupling (J) between the donor and acceptor in the π–π stacked DA pair (DA1) by considering the contribution from both long-range Coulombic coupling (J_{Coul}), and short-range charge-transfer coupling (J_{CT}). The J_{Coul} arising from the interaction between the molecular transition dipole moments was computed using the transition charge from the electrostatic potential (TrEsp) method (see ESI,† Section S1.7).[16] The J_{Coul} value was determined to be 840.77 cm^{-1} at the ωb97xd/def2tzvp level of theory. In general, short-range exciton coupling, J_{CT}, which results from the overlap of wavefunctions on adjacent molecules, has a crucial role in defining the excitonic communication within a CT cocrystal assembly.[17] In the current work, J_{CT} was evaluated by using eqn (S5) (ESI†), where t_h and t_e are the computed hole-transfer coupling and electron-transfer coupling respectively—with t_h originating from the overlap of HOMO–HOMO orbitals, and t_e arising from the overlap of LUMO–LUMO orbitals of the monomers. The co-facial DA pair of PYDB–TCNB cocrystal exhibited a J_{CT} value of 141.78 cm^{-1} with t_e = 157.99 cm^{-1} and t_h = 1238.86 cm^{-1}. Thus, the π–π stacking of the cocrystal facilitated exceptional excitonic communication with a total coupling of J_{Total} = 982.55 cm^{-1} owing to the notable magnitudes of both short-range and long-range couplings.

Furthermore, the distinct photophysical properties of the PYDB–TCNB cocrystal were compared with those of the constituent donor (PYDB) and acceptor (TCNB) crystals. The Kubelka–Munk transformed diffuse reflectance spectra of PYDB and TCNB crystals showed signals spanning from 235 to 365 nm and 208 to 360 nm with absorption maxima at 306 nm and 302 nm, respectively (Fig. S9, ESI†). The PYDB–TCNB cocrystal showed a broad (∼185–580 nm) red-shifted absorption signal with a maximum at ∼325 nm and a shoulder band at 470 nm, explicitly confirming the activation of ground-state charge transfer (Fig. 2a). Having determined the CT character in the ground state, we probed the excited-state spectroscopic characteristics of the PYDB–TCNB cocrystal along with those of PYDB and TCNB crystals. The steady-state emission of PYDB crystal spanned from 380 to 580 nm and revealed emission intensity maximum at λ_{max}^{emi} = 408 nm. Similarly, for the acceptor TCNB, the steady-state emission displayed a wavelength range of 310 nm to 410 nm with λ_{max}^{emi} = 336 nm. As a result of efficient CT integration, the steady-state photoluminescence spectrum of the cocrystal was highly redshifted with respect to those of the donor and acceptor, and spanned from ∼500 to 850 nm with an emission intensity maximum of 577 nm (Fig. 2 and Fig. S10, ESI†). Furthermore, excitation wavelength-dependent emission spectra of the PYDB crystal, TCNB crystal, and PYDB–TCNB cocrystal were recorded, confirming the presence of a single emissive state in the excited state of the respective crystals (Fig. S11, ESI†). To verify the substantial role played by the intramolecular interactions between donor and acceptor in the crystal structure, the PYDB–TCNB cocrystals were dissolved in dichloromethane, and the steady-state emission spectra of the dissolved material at temperatures of 298 K and 77 K were recorded (Fig. S12, ESI†). At room temperature, compared to the emission spectrum of

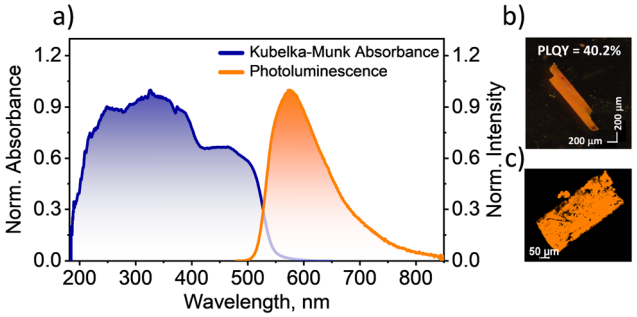

Fig. 2 (a) Normalized Kubelka–Munk transformed diffuse reflectance and photoluminescence spectra, (b) optical image (PLQY = photoluminescence quantum yield), and (c) confocal fluorescence microscopy image (λ_{ex} = 488 nm) of the PYDB–TCNB cocrystal.

the PYDB–TCNB cocrystal in the crystalline state, the solution state exhibited a distinctive difference, showing vibronic bands in the 380–440 nm region, reminiscent of the emission spectra of PYDB. Further cooling the solution using liquid nitrogen to a low temperature facilitated CT complexation and resulted in the emergence of characteristic cocrystal emission bands in the ~515–680 nm regime. This observation further validated the integral function, in the cocrystal, of the cofacial arrangement of donor and acceptor governing the resultant photophysical properties. The confocal fluorescence microscopy image (λ_{ex} = 488 nm), and optical microscopy image were acquired for the PYDB–TCNB cocrystal, and shown in Fig. 2b and c. Subsequently, we performed time-resolved decay measurements to characterize the CT emission from the cocrystal. The photoluminescence lifetime decay profile of the PYDB–TCNB cocrystal was recorded at room temperature by exciting it with 340 nm wavelength nanoLED and collecting the photons at 577 nm. Interestingly, a long-lived excited-state species, with an average lifetime of 37.2 ns, was observed at room temperature at ambient conditions, making plausible a long-lived emission from the CT state of the cocrystal compared to the lifetime of the PYDB donor (4.94 ns) (Fig. S13 and S14, ESI†). The photoluminescence quantum yield (PLQY) measurements of the PYDB–TCNB cocrystal revealed an impressive value of 40.2%.

To confirm the origin and nature of the CT emission, we recorded the steady-state photoluminescence spectrum and the lifetime decay profile of the PYDB–TCNB cocrystal at various temperatures starting from cryogenic conditions (Fig. 3). The steady-state photoluminescence spectrum of the cocrystal exhibited a maximum intensity at a temperature of 90 K, and this intensity diminished along with spectral broadening occurring upon increasing the temperature. The enhanced emission intensity and narrowness of steady-state emission at 90 K can be attributed to the restriction of thermal vibrations leading to the reduced nonradiative pathways in the cocrystal.[18] Having established the CT emission from the PYDB–TCNB cocrystal, the photoluminescence decay profiles were recorded at a low temperature of 20 K to room temperature in a vacuum. The average decay lifetimes were found to be 72.57 ns, 71.27 ns, 66.88 ns, 57.53 ns, and 49.8 ns for 20 K, 100 K, 175 K, 250 K, and 300 K, respectively, at vacuum (Fig. 3b and Table S4, ESI†). The longer decay time at the cryogenic temperature, compared to those at higher temperatures, explicitly confirmed the temperature sensitivity of the emission from the CT state. In vacuum, the room-temperature lifetime was 49.8 ns, higher than the 37.2-ns lifetime at ambient conditions (in the presence of oxygen), hinting at the triplet spin character of the emissive species.[19] For further evaluation, we recorded gated emission spectra of the PYDB–TCNB cocrystal at various temperatures (90 K to 270 K) by exciting the cocrystal with 350 nm wavelength light and with a delay time of 50 μs. The delayed emission spectra spanned in the spectral region similar to the prompt emission and showed an increase in the delayed emission intensity at low temperatures (Fig. S15, ESI†). This result possibly suggested the existence of phosphorescence stemming from the CT state of the PYDB–TCNB cocrystal.[19,20] However, the shorter lifetime possibly suggested the weak nature of phosphorescence emission at low temperatures. Furthermore, fluorescence lifetime imaging (FLIM) analysis of the PYDB–TCNB cocrystals using a MicroTime 200 (MT200) time-resolved fluorescence microscope was conducted to provide a pictorial representation of the fluorescence lifetime. The inverted microscope (Olympus IX83) was equipped with a piezo-scanning stage (P-733.2CD, PI), and the sample was excited using a 404 nm wavelength pulsed laser (LDH-D-C-405, PicoQuant). The FLIM-fitted lifetime was found to be 34.9 ns at ambient

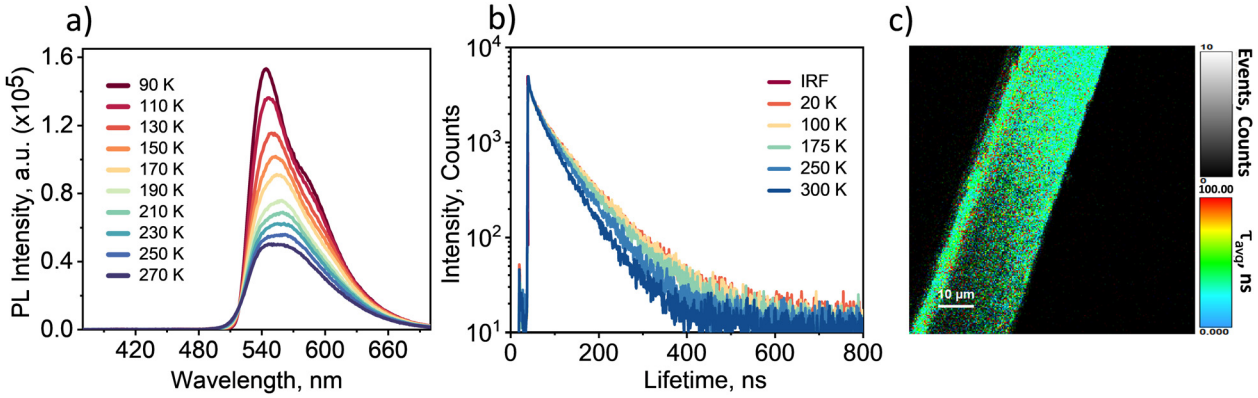

Fig. 3 (a) Steady-state photoluminescence spectra and (b) lifetime decay plots at indicated temperatures and (c) FLIM of the PYDB–TCNB cocrystal.

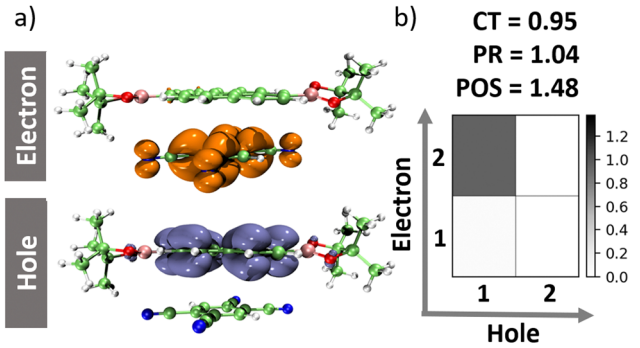

Fig. 4 (a) Hole–electron isosurface distribution for the S_1 state (isovalue = 0.001). (b) Corresponding hole–electron correlation plots showing the CT nature of the S_1 state obtained using TheoDORE analysis at the LC-ωhPBE/6-31G(d,p) level of theory. The CT and PR values are shown to define the nature of excitations.

conditions, in agreement with the decay lifetime of the PYDB–TCNB cocrystal (Fig. 3c and Fig. S16, ESI†).

To gain a deeper understanding of the contribution of the CT in the excited state, fragment-based excited-state analysis, developed by Plasser and implemented in TheoDORE, was performed.[21] The excited-state characteristics were described by participation ratio (PR), charge-transfer character (CT), and mean position (POS) of the initial orbital (hole) and final orbital (electron). In general, CT is correlated with the total weight of configurations in which the initial and final orbitals reside on distinct fragments, where the extreme scenarios CT = 0 and CT = 1 denote the Frenkel state and charge-separated state, respectively (ESI,† Section S1.8). TheoDORE analysis of the S_1 state in the current work was performed by considering the donor and acceptor as two distinct fragments at the LC-ωhPBE/6-31G(d,p) level of theory. The CT value for the S_1 state was determined to be 0.95, confirming the appreciable through-space exciton communication between the donor and acceptor in the cocrystal (Table S5, ESI†). Electron–hole correlation plots in general help to pictorially translate the CT value and uncover the spatial correlation effects. The localization, in the current work, of the hole in the donor and electron in the acceptor illustrated the CT nature (Fig. 4a and b). Similarly, we performed a TheoDORE analysis of the T_1 state, which yielded a CT value of 0.55, also suggesting the CT character (Fig. S17, ESI†). Natural transition orbital (NTO) analysis is in general used to provide a simplistic representation of a complex electronic transition to a major transition.[22] In concurrence with the experimental evidence, NTO analysis of the S_1 state indubitably confirmed the strong CT character by showing spatially separated holes and electrons in the donor and acceptor, respectively (Fig. S18, ESI†). Additionally the visualization of the highest occupied molecular orbital (HOMO) and lowest unoccupied orbital (LUMO) showed the electron density contribution on the donor and acceptor in the HOMO and LUMO, respectively, with stabilizing energy values $E^{HOMO} = -7.922$ eV and $E^{LUMO} = -1.374$ eV further supporting the observations of the NTO analysis (Fig. S18, ESI†).

In summary, we have reported a novel through-space CT cocrystal, PYDB–TCNB, exhibiting a remarkable PLQY and CT emission from the singlet state. Intensified photoluminescence and increased fluorescence lifetime at cryogenic temperature suggested that the emission emanated from the CT state, resulting from the restriction of vibrational motions. A FLIM analysis enabled a pictorial representation of the fluorescence lifetime of the PYDB–TCNB cocrystal. The crucial role of the co-facial organization of donor and acceptor in stabilizing the 3D assembly and influencing the photophysical properties was validated by theoretical calculations, including SAPT, NCI, Hirshfeld, NTO, TheoDORE analysis, long-range Coulombic coupling, and short-range charge-transfer coupling. The present work has elevated the importance of heavy-atom-free organic cocrystals in the field of solid-state emitters for future applications.

Data availability

All the experimental data are provided in the ESI.†

Conflicts of interest

There are no conflicts to declare.

Acknowledgements

M. H. acknowledges MoE-STARS/STARS-2/2023-0770 for financial support. S. S. acknowledges PMRF for financial assistance. We kindly thank Mr Alex P. Andrews for the X-ray diffraction analyses. We thank the Padmanabha HPC cluster at IISER TVM for the computing time. We thank JNCASR Bengaluru for use of the Edinburgh FLS1000 spectrophotometer facility.

References

1 H.-H. Fang, J. Yang, J. Feng, T. Yamao, S. Hotta and H.-B. Sun, *Laser Photonics Rev.*, 2014, **8**, 687–715.
2 A. A. Dar and A. A. Malik, *J. Mater. Chem. C*, 2024, **12**, 9888–9913.
3 L. Sun, W. Zhu, X. Zhang, L. Li, H. Dong and W. Hu, *J. Am. Chem. Soc.*, 2021, **143**, 19243–19256.
4 J. Yang, M. Fang and Z. Li, *Aggregate*, 2020, **1**, 6–18.
5 Y. Zhao, B. Ding, Z. Huang and X. Ma, *Chem. Sci.*, 2022, **13**, 8412–8416.
6 S. Ren, G.-Y. Qiao and J.-R. Wu, *Chem. Soc. Rev.*, 2024, **53**, 10312–10334.
7 A. A. Dar, S. H. Lone, I. Ahmad, A. A. Ahangar, A. A. Ganie and C. Femina, *Mater. Adv.*, 2024, **5**, 1056–1064.
8 J. C. Christopherson, F. Topić, C. J. Barrett and T. Friščić, *Cryst. Growth Des.*, 2018, **18**, 1245–1259.
9 R. Ramakrishnan, M. A. Niyas, M. P. Lijina and M. Hariharan, *Acc. Chem. Res.*, 2019, **52**, 3075–3086.
10 A. R. Mallia, P. S. Salini and M. Hariharan, *J. Am. Chem. Soc.*, 2015, **137**, 15604–15607.
11 R. M. Ipe, A. Parammal, P. Nag, S. Mori, S. R. Vennapusa and S. Gokulnath, *J. Org. Chem.*, 2023, **88**, 5780–5790.
12 A. D. Nidhankar, Goudappagouda, V. C. Wakchaure and S. S. Babu, *Chem. Sci.*, 2021, **12**, 4216–4236.

13 M. A. Spackman and D. Jayatilaka, *CrystEngComm*, 2009, **11**, 19–32.
14 J. Contreras-García, E. R. Johnson, S. Keinan, R. Chaudret, J.-P. Piquemal, D. N. Beratan and W. Yang, *J. Chem. Theory Comput.*, 2011, **7**, 625–632.
15 C. D. Sherrill, *Acc. Chem. Res.*, 2013, **46**, 1020–1028.
16 S. Soldner, O. Anhalt, M. B. Sárosi, M. Stolte and F. Würthner, *Chem. Commun.*, 2023, **59**, 11656–11659.
17 N. J. Hestand and F. C. Spano, *J. Chem. Phys.*, 2015, **143**, 244707.
18 S. Garain, S. N. Ansari, A. A. Kongasseri, B. Chandra Garain, S. K. Pati and S. J. George, *Chem. Sci.*, 2022, **13**, 10011–10019.
19 A. A. Kongasseri, S. N. Ansari, S. Garain, S. M. Wagalgave and S. J. George, *Chem. Sci.*, 2023, **14**, 12548–12553.
20 A. A. Kongasseri, S. Garain, S. N. Ansari, B. C. Garain, S. M. Wagalgave, U. Singh, S. K. Pati and S. J. George, *Chem. Mater.*, 2023, **35**, 7781–7788.
21 F. Plasser, *J. Chem. Phys.*, 2020, **152**, 084108.
22 R. L. Martin, *J. Chem. Phys.*, 2003, **118**, 4775–4777.

